

Ab initio* self-consistent study of the electronic structure and properties of cubic boron nitrideAlex Zunger[†] and A. J. Freeman*Department of Physics and Astronomy, and Materials Research Center, Northwestern University, Evanston, Illinois 60201*

(Received 4 May 1977)

We present the results of a first-principles fully self-consistent study of the electronic properties of cubic boron nitride in the local-density formalism using our previously published numerical-basis-set linear combination of atomic orbitals scheme. The resulting band structure shows considerable disagreement with previously published orthogonalized-plane-wave, augmented-plane-wave, and pseudopotential studies. A detailed study of the *ground-state* properties of the system, such as x-ray scattering factors, cohesive energy, equilibrium lattice constant, and their behavior under pressure, yields very good agreement with available experimental data. Reasonably good agreement is obtained for *excited state* properties determined by optical and x-ray absorption measurements. The bonding characteristics in this prototype of III-V compounds are discussed in detail and compared with results of our previous study of its isoelectronic homopolar analog, diamond, and with studies on the hexagonal graphite-like modification of BN.

I. INTRODUCTION

The extraordinary properties of cubic boron nitride have been the subject of intense experimental investigations since its discovery in 1957 by Wentorf.¹ The simplest III-V compound, it is isoelectronic and isostructural with diamond. Its hardness matches that of diamond² while its effective ionic charge is the highest of all known III-V compounds.^{3,4} Like carbon, BN crystallizes in two forms, a cubic zinc-blende and an hexagonal (graphite-like) structure. These properties make a comparative study of these compounds particularly interesting. We have previously studied the electronic properties of diamond^{5,6} in the local-density formalism (LDF)^{7,8} using our first-principles self-consistent numerical-basis-set linear combination of atomic orbitals (LCAO) method.^{9, 10} In particular, we have investigated the band structure, charge distribution (as measured by x-ray scattering factors), cohesive energy, equilibrium lattice constant, behavior under pressure, and the bonding characteristics induced by the various electron exchange and correlation potentials pertaining to the local-density formalism. In this study, we extend our investigation to the isoelectronic cubic boron nitride in an attempt both to understand the electronic structure features in the heteropolar zinc-blende system and to test further the applicability of the LDF to quantitative descriptions of covalent-ionic systems.

The crystal structure of cubic boron nitride has been established by Wentorf¹ (lattice constant $a = 3.615 \pm 0.001$ Å at 25 °C). Its optical properties in the infrared region have been studied by Gieliisse *et al.*³ and recently by Chrenko¹¹ who has also investigated its ultraviolet absorption spectra. Some preliminary results have also been published by Phillip

and Taft¹² and Halperin and Katzir.¹³ The spectra of the core levels have been studied by means of x-ray emission spectroscopy.¹⁴⁻¹⁶ The distribution of electrons in the ground state recently has been studied by Weiss¹⁷ by means of x-ray crystallography.

Theoretical studies¹⁸⁻²⁷ of the electronic structure of cubic BN include the work of Kleinman and Phillips¹⁸ using a pseudopotential technique in which the heteropolar antisymmetric potential (which vanishes in the homopolar diamond case),¹⁹ is treated as a small perturbation on the previously computed diamond potential. Hamstreet and Fong²⁶ have indicated that since the basic pseudopotential cancellation in crystals like BN made up of first-row atoms is incomplete due to the lack of p character in the core states, a nonlocal correction to the pseudopotential is necessary. Adjusting empirically their local and nonlocal pseudopotential parameters, they obtained a band structure that differs substantially from that of Kleinman and Phillips.¹⁸ In a subsequent orthogonalized-plane-wave (OPW) study, Bassani and Yoshimine²² have similarly faced a plane-wave convergence difficulty due to the lack of pseudopotential cancellation for crystal states having p symmetry. (Their model employs atomic *Hartree-Fock* charge densities to represent the crystalline density and the crystal exchange potential is linearized with respect to the single-site potentials). Wiff and Keown²³ and Keown²⁴ have calculated the band structure of BN using the augmented-plane-wave (APW) method with a muffin-tin crystal potential in which the boron and nitrogen potentials were obtained by linearly scaling the carbon potential and adding a constant Madelung term (with effective charge chosen empirically to yield a gap of 8.8 eV)³ to account for the partial ionic character of the system.

TABLE I. The prediction of energy separation between high-symmetry points in the zone given by various band models: Δ_{\min} indicates the lowest point in the conduction band in the Γ - X direction; WVB1 and WVB2 refer to the width of the lowest (VB1) and highest (VB2) valence bands, respectively, and WVB is the total width of the occupied valence band. Results are given in eV. Asterisks denote values interpolated from the published figures.

Energy difference	Emp. ^a	APW ^b	OPW ^c	Pseudo ^d	Present exchange and correlation
$\Gamma_{15,v} \rightarrow \Gamma_{15,c}$	10.8	8.9	7.6	14.3	10.8
$\Gamma_{15,v} \rightarrow \Gamma_{1,c}$	8.4	9.6	8.4	20.0	11.9
$L_{3,v} \rightarrow L_{1,c}$	9.9	11.2	13.4	14.4	14.2
$X_{5,v} \rightarrow X_{3,c}$	13.8	14.5	13.6*	14.7	18.7
$X_{5,v} \rightarrow X_{1,c}$	12.7	13.3	9.0	13.4	12.9
$L_{3,v} \rightarrow L_{3,c}$	15.0	11.7	11.8	15.4	15.4
$\Gamma_{15} \rightarrow \Delta_{\min}$	7.6	7.2	3.0	10.5	8.7
WVB	27.5	17.8	23.2	17.9	19.1
WVB1	6.8*	4.5	5.0*	5.6	5.1
WVB2	16.5	8.0	12.7*	3.5	9.0

^a Empirical (nonlocal) pseudopotential, Ref. 26.

^b Reference 23.

^c Reference 22.

^d Perturbative pseudopotential, Ref. 19.

Table I presents the energies of the lowest inter-band transitions at high symmetry points, the width of the lowest valence bands (VB1 and VB2, respectively) and the total width of the occupied bands predicted by these four models. The agreement between these results is seen to be generally very poor. The two nonempirical studies (OPW)²² and pseudopotential¹⁸ yield results that differ by as much as 6.7 eV for the direct gap, 7.5 eV for the indirect gap, and 5.3 eV for the valence band width. The APW^{23,24} and the empirical pseudopotential²⁶ studies which use empirical parameters, as well as the early semiempirical LCAO studies of Coulson *et al.*²⁰ and Redei²¹ yield similarly very inconclusive and scattered results. This demonstrates the inherent difficulties in obtaining a reliable theoretical model for a compound like BN in which the degree of interatomic charge transfer is intermediate between the purely covalent and purely ionic limits and a straightforward plane-wave expansion of the crystal potential is very slowly convergent²⁸ on account of the absence of p character in the core orbitals.

In the present study, we use a first-principles approach in which the crystal potential is determined self-consistently with no *ad-hoc* assumptions and the band Hamiltonian is solved in an extended LCAO set to determine the band structure, charge density, behavior under pressure, and cohesive properties. The bonding mechanism in BN is discussed in detail and the results compared with those obtained in our previous study on diamond,⁵ and with studies on the hexagonal form of BN.^{29,30}

II. METHODOLOGY: THE SELF-CONSISTENT CRYSTAL POTENTIAL

As a first step toward the determination of the self-consistent (SC) crystal potential in the local-density formalism, we construct a model charge density. The individual α -site densities $\rho_{\alpha}(\vec{r})$, $\{f_{nl}^{\alpha} Q^{\alpha}\}$ obtained from the SC solution of the *atomic* local-density equation for the assumed central field (nl) orbital occupation numbers f_{nl}^{α} and ionic charge Q^{α} are lattice summed to yield the population-dependent superposition density $\rho_{\text{sup}}(\vec{r}, \{f_{nl}^{\alpha}, Q^{\alpha}\})$. For the particular case where the $\{f_{nl}^{\alpha}, Q^{\alpha}\}$ are chosen as the populations and charges of the ground state atoms, $\rho_{\text{sup}}(\vec{r}, \{f_{nl}^{\alpha}, Q^{\alpha}\})$ constitutes a superposition of overlapping undistorted single-site densities. This quantity is then used to generate the various components of the local-density crystal potential: the short-range Coulomb part $V_{\text{SRC}}^{\text{sup}}(\rho_{\text{sup}}(\vec{r}))$ is obtained by solving the associated Poisson equation and similarly the first approximation to the exchange-correlation potential $V_{\text{xc}}^{\text{sup}}(\rho_{\text{sup}}(\vec{r}))$ is obtained by applying the corresponding local-density functionals^{7,8,31} directly to $\rho_{\text{sup}}(\vec{r})$. After the lattice summation leading to $V_{\text{SRC}}^{\text{sup}}(\rho_{\text{sup}}(\vec{r}))$ is completed at a large cut-off distance (17 a.u.), there still remains a long-range electrostatic "tail" to each of the atomic Coulomb potentials due to the unscreened ionic charge Q^{α} . The potential due to a lattice of such point charges is then calculated by the Ewald method³² to yield the long-range Coulomb term $V_{\text{LRC}}^{\text{sup}}(\vec{r})$. Our initial crystal potential $V^{\text{sup}}(\rho_{\text{sup}}(\vec{r}))$ is given as the sum

of $V_{\text{SRC}}^{\text{sup}}(\rho_{\text{sup}}(\vec{r})) + V_{\text{xc}}^{\text{sup}}(\rho_{\text{sup}}(\vec{r})) + V_{\text{LRC}}^{\text{sup}}(\vec{r})$ and depends on the assumed set $\{f_{ni}^{\alpha}, Q^{\alpha}\}$ for boron and nitrogen and on the lattice structure. The initial guess for these populations is the neutral atom configurations $\text{B}^{\circ} 1s^2 2s^2 2p^1$ and $\text{N}^{\circ} 1s^2 2s^2 2p^3$. The potential is calculated in tabular form over a set of 3500 integration points in the unit cell. Linearization²² of $V_{\text{xc}}(\rho_{\text{sup}}(\vec{r}))$ with respect to the atomic densities $\rho_{\alpha}(\mathbf{r})$ is avoided, and similarly, no use is made of spherical approximations^{23,24} to the total potential $V^{\text{sup}}(\rho_{\text{sup}}(\vec{r}))$.

We solve the band problem with this initial potential in the LCAO representation using our previously published numerical-basis-set discrete-variational technique.^{9,10} We use as basis functions Bloch states $\Phi_{\mu\alpha}(\vec{k}, \vec{r})$ formed from accurate numerical solutions $\chi_{\mu}^{\alpha}(\mathbf{r})$ to the atomic-local-density equations, again with an assumed population and charges $\{f_{ni}^{\alpha}, Q^{\alpha}\}$. We use numerical orbitals corresponding to $\mu = 1s, 2s, 2p, 3s,$ and $3p$ for both boron and nitrogen; the addition of $3d$ orbital was found to introduce negligible changes in the band structure for energies lower than 16 eV above the valence band edge.

The Hamiltonian matrix elements in the Bloch basis are computed by a three-dimensional Diophantine integration scheme³³ and include all the multicenter integrals up to an interatomic separation distance of 16.5 a.u. This summation range, together with the use of 3500 Diophantine integration points, assures a stability of 0.05–0.1 eV in the band eigenvalues in the energy range studied. The band Hamiltonian is solved for 10 special points in the irreducible Brillouin zone (BZ)³⁴ and the resulting crystal wave functions at these points are used to generate the output density, $\rho_{\text{cry}}(\vec{r})$. A smaller set of 6 special BZ points (Γ - X - L - W - Δ - Σ) produced a charge density that differs by less than 1% from that determined by the 10-point sampling. The output crystal density $\rho_{\text{cry}}(\vec{r})$ differs, in the general case, from our model density $\rho_{\text{sup}}(\vec{r}, \{f_{ni}^{\alpha}, Q^{\alpha}\})$ both due to the *intra-atomic* charge redistribution (e.g., promotion of nitrogen $2s$ charge into the nitrogen $2p$ shell) and due to charge flow *between* the atoms. To take account of these effects, we use our charge and configuration SC (CCSC) procedure.¹⁰ We hence minimize the difference $\Delta\rho(\vec{r}) = \rho_{\text{sup}}(\vec{r}, \{f_{ni}^{\alpha}, Q^{\alpha}\}) - \rho_{\text{cry}}(\vec{r})$ over the unit-cell space in the least squares sense by iteratively varying the set of orbital populations and charges $\{f_{ni}^{\alpha}, Q^{\alpha}\}$, and recalculate the new single-site densities $\rho_{\alpha}(\mathbf{r}, \{f_{ni}^{\alpha}, Q^{\alpha}\})$, the basis function $\chi_{\mu}^{\alpha}(\vec{r})$ and crystal potential $V^{\text{sup}}(\rho_{\text{sup}}(\vec{r}, \{f_{ni}^{\alpha}, Q^{\alpha}\}))$, correspondingly.

Figure 1 shows the quantity $\Delta\rho(\vec{r})$ obtained after the first iteration (full line) along the bonding $[111]$ direction. Along with some buildup of density in

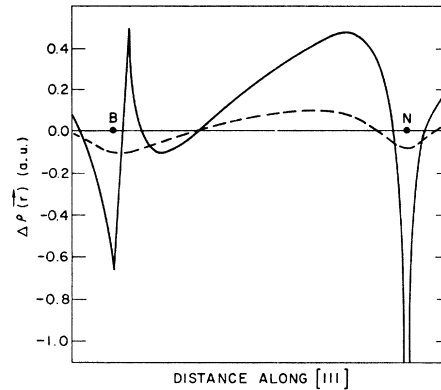


FIG. 1. Charge-density difference, $\Delta\rho(\vec{r})$ in a.u., between the values obtained in the superposition model and the crystal densities obtained at the first CCSC iteration (full line) and at the convergence limit of the CCSC iterations (dashed line).

the interatomic region (indicating some covalent bond formation), there appear additional sharp features on the atomic sites themselves due to the accumulation of extra charge on the electronegative nitrogen atom and some change in the positions of the boron orbital nodes relative to the superposition limit. The dashed line in this figure represents the *residual* $\Delta\rho(\vec{r})$ obtained after six iterations. The final electronic configuration obtained in this way is $\text{B } 1s^{2.00} 2s^{0.65} 2p^{1.75} 3s^{0.12} 3p^{0.13}$ and $\text{N } 1s^{2.00} 2s^{1.71} 2p^{3.52} 3s^{0.08} 3p^{0.04}$ corresponding to formal net charges of $\text{B}^{+0.35} \text{N}^{-0.35}$. This configuration indicates some $2s$ to $2p$ intra-atomic charge transfer together with a transfer of electronic charge from the boron s shell to the nitrogen p shell and some population of the formerly unoccupied atomic $3s$ and $3p$ orbitals.

Although this final CCSC configuration constitutes an “optimal” choice within the basis of exact local density atomic densities, it does not simulate the output crystal density $\rho_{\text{cry}}(\vec{r})$ very accurately; a standard deviation of about $0.10e$ (out of 12 unit-cell electrons) still marks a substantial difference between the refined superposition density and the variationally obtained $\rho_{\text{cry}}(\vec{r})$. Thus, there are still non-negligible parts of the crystal density that are not amenable to accurate representation by a superposition of optimized atomic-like densities located around existing atomic sites. To account for this residual density we proceed to the second step in self-consistency (“full SC”) by Fourier transforming the *residual* $\Delta\rho(\vec{r})$ over a set of reciprocal-lattice vectors (RLV) and solving the associated Poisson equation directly in reciprocal space.⁹ Owing to the smooth character of the final $\Delta\rho(\vec{r})$ (cf. Fig. 1), such a Fourier series converges rather rapidly (the first 12 stars

are needed) and does not give rise to the usual convergence difficulties associated with the Fourier decomposition of the *all-electron* (core plus valence) density.^{35,36} The correction $\Delta V(\vec{r})$ to the Coulomb interelectronic potential thus obtained is added to the crystal Coulomb potential obtained in the last CCSC iteration while the refined exchange-correlation potential $V_{\text{xc}}(\rho_{\text{cry}}(\vec{r}))$ is calculated directly from $\rho_{\text{sup}}(\vec{r}) + \Delta\rho(\vec{r})$. The new Hamiltonian is diagonalized repeatedly to obtain finally a negligible $\Delta\rho(\vec{r})$ (i.e., $\int |\Delta\rho(\vec{r})| dr \leq 10^{-3}e$) between successive iterations.

The final crystal potential is plotted in Fig. 2 along the $[111]$ bond direction. It is seen that the exchange potential constitutes some 40% of the Coulomb potential in the bond center region while the correlation part is one order of magnitude smaller. Both exchange and correlation parts become negligible relative to the Coulomb part at distances of about 0.2 a.u. from the nuclei. The long-range electrostatic potential is seen to have large nonconstant contributions in the bond region and acts to stabilize the more electronegative nitrogen site relative to the boron site.

Figure 3 shows the difference in the various potential components between diamond⁵ and BN along the $[111]$ direction. Both the short-range and the long-range Coulomb potentials give rise to rather sizable asymmetric contributions to the potential difference while the exchange and correlation terms are less asymmetric. The sizable lowering of the potential near the nitrogen site causes an appreciable charge flow to this region and increases the polarity of the system. These appreciable differences in the SC potentials of diamond and BN

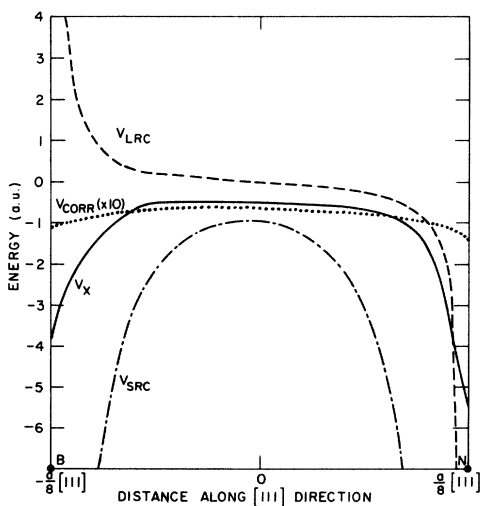


FIG. 2. Contributions to the self-consistent crystal potential in cubic BN along the bonding $[111]$ direction. Note the change in scale for V_{corr} .

seem to suggest that a first-order perturbation^{18,37} in ΔV would not suffice to quantitatively describe the accompanying differences in their band structure. In particular, we find that the ratio between the asymmetric potential Fourier coefficients for the (111) and (200) reflections is about a factor of 2 smaller than that obtained by Kleinman and Phillips¹⁸ in their perturbative treatment.

III. RESULTS

A. Band structure

The band structure of cubic boron nitride was calculated with the final SC potential at $24 \vec{k}$ points in the irreducible zone. Figure 4 shows the results obtained for an exchange only model (i.e., without the correlation potential³¹) using an exchange coefficient α of $\frac{2}{3}$ and 1. On the right-hand side we have indicated by horizontal lines the corresponding free-ion eigenvalues.

The valence band of cubic BN is split into two parts: a lower (VB1) band and a group of three higher bands (VB2) separated by a gap of 4.7 and 5.0 eV for $\alpha = \frac{2}{3}$ and 1 respectively. The bands are slightly wider with $\alpha = \frac{2}{3}$ (5.3 and 9.2 eV for VB1 and VB2, respectively) than with $\alpha = 1$ (4.9 and 8.9 eV, respectively). The VB2 band edge ($\Gamma_{15, \nu}$) is separated from the conduction bands by an indirect gap of 8.5 eV ($\alpha = \frac{2}{3}$) and 8.8 eV ($\alpha = 1$), while the direct $\Gamma_{15, \nu} - \Gamma_{15, c}$ gap is 10.7 and 11.2

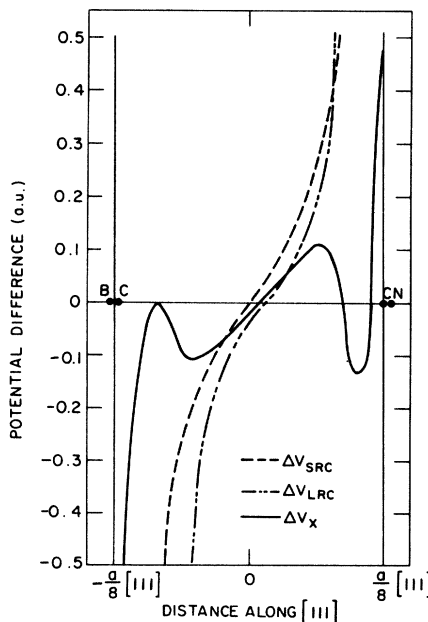


FIG. 3. Differences between components of the self-consistent diamond (Ref. 5) and BN potentials. The black dots mark the positions of the atoms along the $[111]$ direction.

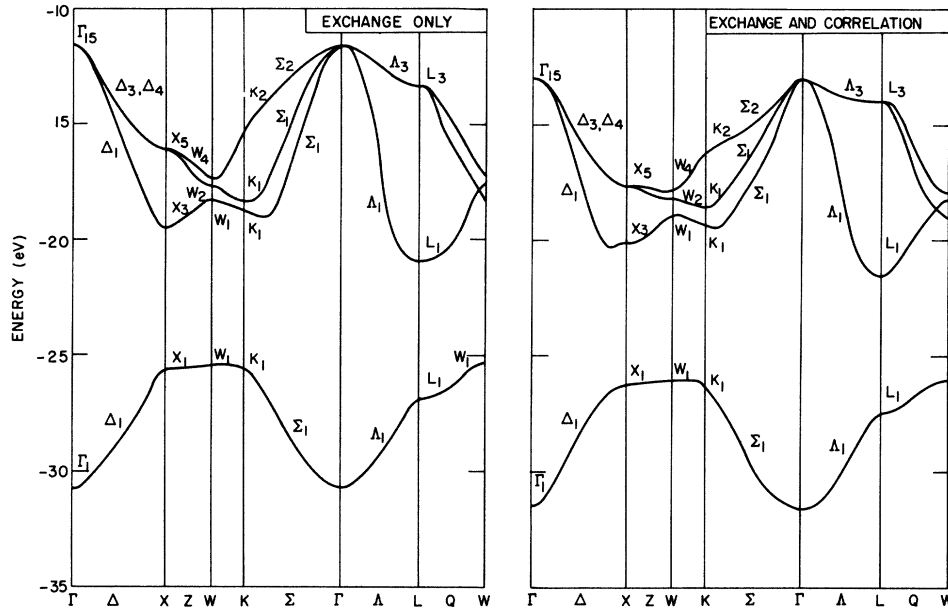


FIG. 5. Valence band structure of cubic BN in the exchange model ($\alpha = \frac{2}{3}$) and in the exchange and correlation model ($\alpha = \frac{2}{3}$).

B-N LCAO's are permitted by symmetry for the $\Gamma_{15,v}$ and $X_{1,c}$ band edge states in the zinc-blende structure, the P_1^- and P_2^- hexagonal states are Bloch states constructed either of N or B orbitals and hence the gap is purely heteropolar. (In the homopolar graphite analog, this gap reduces to zero due to the inversion symmetry associated with the equivalent atoms in the unit cell, and gives rise to its semimetallic properties.) The lattice constant dependence (e.g., pressure changes or temperature effects) of the band gap in hexagonal BN is hence expected²⁹ to be much weaker than the corresponding dependence in cubic BN on account of the occurrence of two-center interaction terms in the $\Gamma_{15,v} \rightarrow X_{1,c}$ transition energy as opposed to the appearance of one-center (boron and nitrogen) terms in the analogous transition in the hexagonal modification.

The calculated value for the $K_{2,v} \rightarrow K_{1,c}$ transition energy (14.6 eV) and the $X_{5,v} \rightarrow X_{1,c}$ energy (12.9 eV) are in good agreement with the large peak observed at 14.5 eV and its low energy shoulder at about ~13 eV. The transitions between these states form the fundamental optical band in a large number of III-V zinc-blende materials,³⁹ the energies of these transitions decreases monotonically with the increase in electronegativity difference of the constituent atoms.

The width of the valence band of BN has been measured by Formichev and Rumsh¹⁶ to be 15.4–22 eV, a value which brackets our value of 19.1 eV. The remaining data of Table I still await experimental verification.

Upon comparing our results for BN with those

previously obtained by the same method for diamond,⁵ we note an increase in the ionization energy (from 10.5 to 11.9 eV) and a decrease in the band width (20.4 to 19.1 eV). Similarly the indirect Γ - Δ gap increases from 5.45 eV in diamond to 8.7 eV in BN and the leading L gaps ($L'_{3,v} - L'_{1,v}$ and $L'_{3,v} - L_{3,c}$) increase from 13.3 and 13.2 eV in diamond to 14.2 and 15.4 eV in BN, respectively. These trends are consistent with the increased ionicity of BN relative to the covalent diamond case.^{39,40} The low-lying conduction bands at the X -point ($X_{1,c}$ and $X_{3,c}$) in BN are split while in diamond they are degenerate ($X_{1,c}$). The magnitude of this splitting (5.8 eV) is larger than that obtained in the perturbative pseudopotential study¹⁸ (1.36 eV) but is comparable to the results obtained in the OPW²² and APW²³ studies (4.76 and 3.7 eV, respectively), and is responsible in part for the lower gap obtained here relative to the pseudopotential study. We find that the magnitude of the $X_{1,c}$ to $X_{3,c}$ splitting obtained here is rather insensitive to addition of more diffused basis functions (e.g., the plane-wave-like $3d$ orbitals) and hence the deviation obtained from other calculations are not due to difficulties associated with the use of an "atomic-like" representation.

B. Charge density

To study the bonding mechanism in cubic BN, we first consider the orbital nature of the occupied bands. Figures 6 and 7 show the orbital charge density along the $[111]$ direction of some high-symmetry states in VB1 and VB2, respectively. The

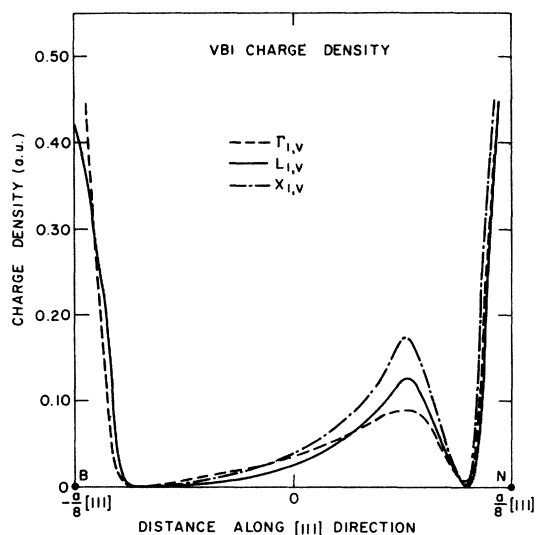


FIG. 6. Orbital charge densities of some high symmetry states in the lower valence bands (VB1) along the [111] direction. The atomic positions are indicated by full dots.

$\Gamma_{1,v}$ point at the bottom of VB1 is a hybrid between N and B $2s$ orbitals with a somewhat larger proportion of the former; the higher-lying $L_{1,v}$ point in VB1 contains some B $2p$ character and only a small B $2s$ admixture resulting in an enhanced density in the bond region. Finally, the $X_{1,v}$ point at the top of VB1 is a N s -B p hybrid which has appreciable amplitude only in the N region. In the VB2 group of bands one finds an N p -B sp hybrid at the bottom $X_{3,v}$; at $L_{1,v}$, the B s character de-

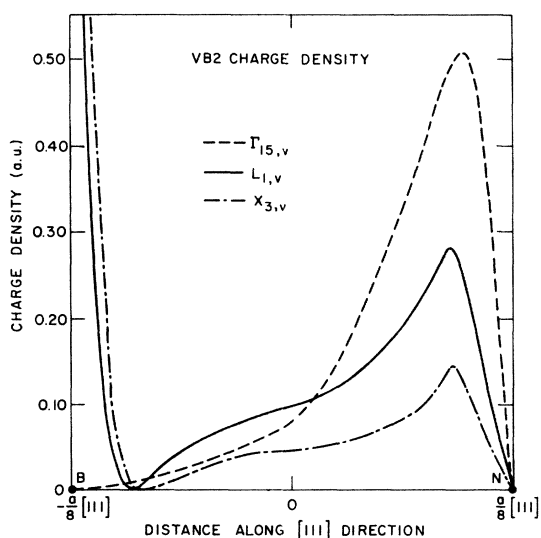


FIG. 7. Orbital charge densities of some high symmetry states in the upper valence bands (VB2) along the [111] direction.

creases in favor of N $2p$ character; at $\Gamma_{15,v}$ (top of the band) an almost-pure N $2p$ state is formed. The general pattern of orbital densities in VB1 and VB2 shows a charge buildup in the bond region characteristic of covalent bonding together with enhanced amplitudes in the nitrogen region, indicating some ionic character.

A more detailed description of the orbital character throughout the BZ can be obtained by performing a population analysis^{5,41,42} on the crystal wave function. Such a procedure can be conveniently carried out in the Löwdin technique⁴² in which one orthogonalizes the Bloch basis set for different orbital indices μ using a symmetric transformation and identifies the square of the Bloch basis-set coefficients $[C_{\mu\alpha j}(\vec{k})]$ in the LCAO expansion with the μ th orbital charge on site α due to band state $|\vec{k}, j\rangle$. Figure 8 shows the BZ dispersion of the orbital charges summed separately over the band index j of the lower group of valence bands (VB1) and the upper group (VB2). These dispersion curves measure the contribution of each of the basis orbitals to the total ground state charge in each of these valence bands. It is seen that VB1 is a predominantly N $2s$ band having some admixture of B $2p$ character. The degree of hybridization varies considerably across the BZ from a strong N $2s$ -B $2p$ hybrid along X - W - K to a N $2s$ -B $2s$ hybrid at Γ - L . The upper valence band VB2, on the other hand, is almost entirely of pure N $2p$ character with only a slight amount of B $2p$ char-

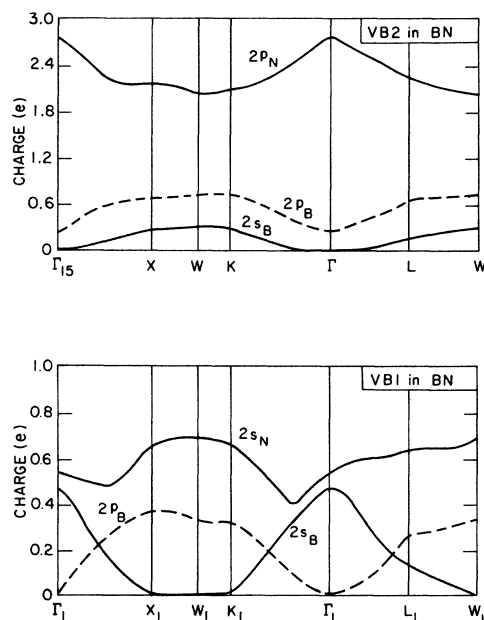


FIG. 8. Dispersion of the orbital charges $q_{\mu\alpha j}(\vec{k})$ in the lower (VB1) and upper (VB2) valence bands of cubic BN.

acter admixed in along the X - W - K directions. These trends are borne out by examining the location of the free-ion eigenvalues on the scale of the band structure (cf., Fig. 4). The N $2s$ eigenvalue has its energy substantially lowered in the solid (to the VB1 region) due to the attractive Madelung well on this negative site. Similarly, a Madelung stabilization of the N $2p$ level lowers its energy into the VB2 bands while the positive-site B $2s$ and $2p$ levels are pushed higher in energy (towards the conduction bands) and thus their admixture into the VB2 bands is diminished.

A description of the orbital character in the entire occupied manifold is given by the BZ dispersion of

$$q_{\mu\alpha}(\vec{k}) = \sum_j^{ooc} q_{\mu\alpha j}(\vec{k})$$

shown in Fig. 9 together with the dispersion of the net ionic charge $Q_{\alpha}(\vec{k}) = Z_{\alpha} - \sum_{\mu} q_{\mu\alpha}(\vec{k})$, where Z_{α} is the α -site atomic number. The striking feature

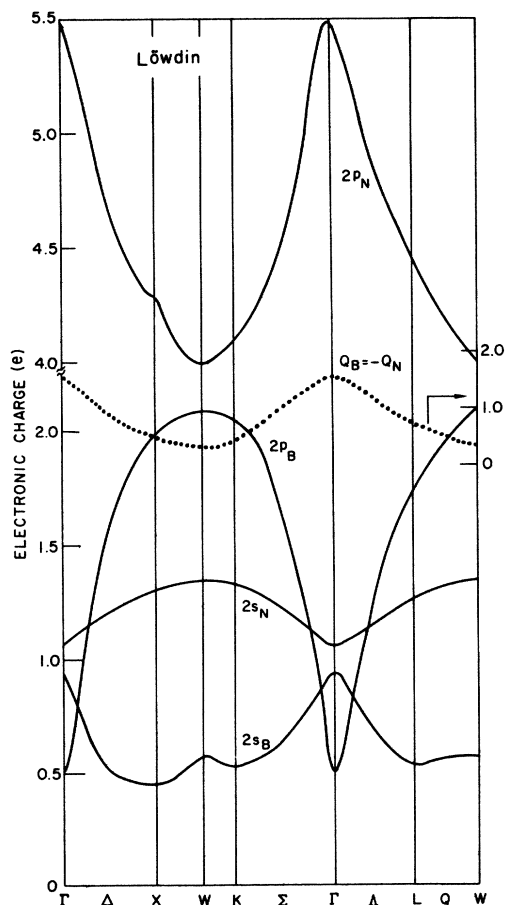


FIG. 9. Dispersion of the Löwdin ground state orbital charges $q_{\mu\alpha}(\vec{k})$ in cubic BN. The dotted line represents the dispersion of the net charges, $Q_{\alpha}(\vec{k})$.

of these results is the substantial variation in orbital character across the zone: while at the Γ point there is a large degree of N $2p$ character with only minor B $2p$ admixture [which results in a large charge polarization of $Q_B(\Gamma) = -Q_N(\Gamma) = 1.55e$], the situation is reversed in the X - W - K directions and this leads to a low average polarity [$Q_B(X-W-K) = -Q_N(X-W-K) = 0.45e$]. Thus, it is clear from the above discussion that a simple assignment of a unique orbital character to any subgroup of bands^{20,21} is impossible. Similarly, the assignment of a constant s to p hybridization ratio to all states in the zone, as is currently done in bond orbital methods,^{43,44} seems very crude.

Before leaving the subject of the orbital character of the bands, some word of caution is in order. Any partitioning of the three-dimensional charge density into orbital contributions associated with particular sites in the solid is not unique and involves a considerable reduction in the information available from the calculated band structure. Among the alternative partitioning methods, we note the Mulliken analysis⁴¹ commonly used in molecular structure calculations⁴⁵ and the partial-wave muffin-tin partitioning used in APW⁴⁶ and multiple-scattering (MS $X\alpha$) methods.⁴⁷ While the square of the wave-function expansion coefficient on a given atomic site can be unambiguously assigned as a contribution of orbital density to this site, the partitioning of cross terms (involving coefficients of more than one site) is rather arbitrary. Whereas, in the Mulliken technique such terms are apportioned equally between the constituent atoms (and hence one neglects any possible electronegativity difference), such terms do not occur in the Löwdin technique because of the orthogonality of the basis. Although, both techniques yield virtually the same results^{9,10} in homopolar systems like diamond, having medium to small intersite overlap, substantial differences may occur in heteropolar systems like BN. To demonstrate this point, we show in Fig. 10 the BZ dispersion of the calculated Mulliken charges in BN. While the general pattern of orbital hybridization is similar to that obtained by the Löwdin method (Fig. 9) quantitative differences do occur; the Mulliken analysis generally yields an enhanced charge polarization (e.g., charges of $Q_B(\Gamma) = -Q_N(\Gamma) = 2.16e$ and an average of $0.86e$ along X - W - K) and a lower BZ orbital charge dispersion. Note, however, that both the Löwdin and the Mulliken schemes do not involve any shape approximation to the variational crystal charge density, contrary to the situation encountered in the partial-wave muffin-tin orbital analysis^{46,47} in which a spherical muffin-tin averaging of the crystal density is performed.

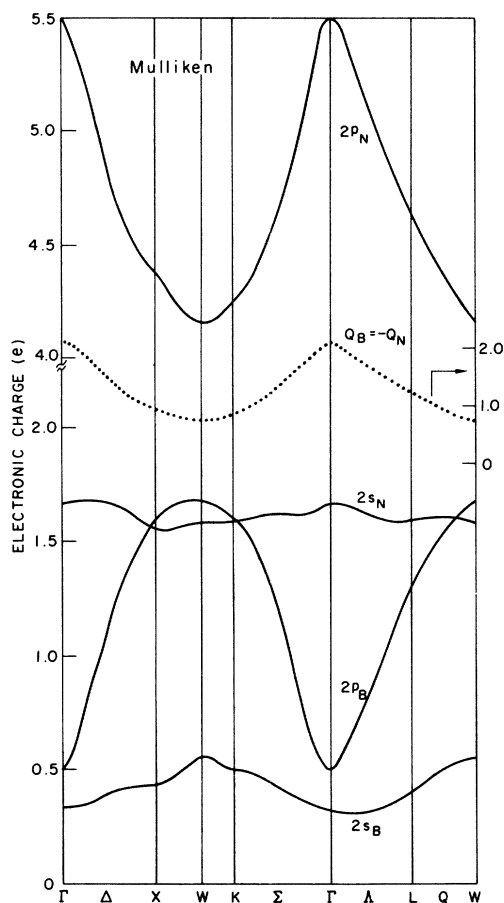


FIG. 10. Dispersion of the Mulliken ground state orbital charges $q_{\mu\alpha}(\vec{k})$ in cubic BN. The dotted line represents the dispersion of the net charges, $Q_{\alpha}(\vec{k})$.

C. Effective charges

It is clear from the above that although a *static* partitioning of the crystal density into the atoms constituting the bond in BN can elucidate the nature of the hybridization and charge transfer, it does not lead to a unique picture of the ionic charges. Moreover, such an approach does not distinguish between an actual transfer of charge and a simple overlap of the orbitals of neighboring atoms. In order to study the *dynamical* aspects of charge transfer, we have calculated the effective charge $e_{\vec{k}}^*$. Here, one expands the crystal dipole moment in the atomic displacement in a standard fashion⁴⁸ and obtains to second order that the $\vec{q} = 0$ displacement mode in the [111] tetrahedral directions [i.e., displacements of $d_+ = -d_- = \frac{1}{8}a(\delta, \delta, \delta)$ where plus and minus refer to the two unit cell ions and δ is the displacement amplitude] yields the effective charge⁴⁹:

$$e_{\vec{k}}^* = 4 \lim_{\delta_{\lambda} \rightarrow 0} \frac{M_{\lambda}}{\delta_{\lambda}}, \quad (1)$$

where the unit cell dipole moment for direction λ is given by:

$$\vec{M}_{\lambda} = \frac{1}{N} \sum_{l\alpha} Z_{\alpha}(\vec{r}_{\lambda l\alpha} + \vec{d}_{\lambda\alpha}) - e \int \vec{r}_{\lambda} \tilde{\rho}(\vec{r}) d\vec{r}. \quad (2)$$

Here, $\vec{r}_{\lambda l\alpha}$ refers to the λ component of the vector joining the origin with the site α in the unit cell l , $\vec{d}_{\lambda\alpha}$ is the λ component of the α -site displacement, and $\tilde{\rho}(\vec{r})$ denotes the variational electronic crystal density obtained for equilibrium unit cell parameters but for atoms displaced along the symmetry preserving directions indicated above.

By repeating the band-structure calculation for three sets of atomic positions related by the $\pm \frac{1}{8}a(\delta, \delta, \delta)$ displacements (with $\delta = 0.001$), integrating numerically the corresponding unit cell dipole moments over a constant (minimum) potential surface and replacing the limit in Eq. (1) by a finite difference, we obtain an effective transverse charge $e_{\vec{k}}^*(B) = -e_{\vec{k}}^*(N) = 2.85e$. This result, which is rather insensitive to small variations in δ , is stable to within 2% when 3000 Diophantine integration points are used and is rather close to the experimental estimate given by Lucovsky *et al.*⁴ ($2.47e$). Such a large value of $e_{\vec{k}}^*$ indicates that, contrary to the rather low ionicity inferred from the static CCSC calculation ($B^{0.35}N^{-0.35}$), dynamically more than 90% of the valence charge is polarized when the atoms are displaced in an optical mode. *Static* ionic charges inferred from bond orbital schemes^{20,50} (in which the ionic charge is determined from the mixing coefficient of the B and N sp^3 hybrid into the ground state, assuming a constant s - p hybridization ratio for all states) yielded values in the range of $0.26e$ - $0.50e$ (with polarity B^+N^-). Our *dynamic* calculation yields a unit cell dipole moment of 4.98 Debye at equilibrium which is substantially larger than the calculated dipole moment of the diatomic BN molecule (~ 2.3 Debye⁵¹) and suggests larger polarization to occur in the solid.

Our charge and configuration study suggests that the intra-atomic charge redistribution effects (i.e., the change in p to s populations from the free-atom values of 0.5 and 1.5 in B and N, respectively to 2.69 and 2.06, respectively, in the CCSC limit) are dominant over the interatomic charge-transfer effects ($0.35e$). Since these charge redistribution effects are not observables, it is difficult to assess the validity of this result. However, it is interesting to note that the study of Kuplyauskis and Yakimavichyus⁵² indicated that only the atomic B and N wave functions corresponding to an sp^3 *intra-atomic* valence excitation, similar to that obtained

here, are capable of reproducing the observed Compton profile¹⁷; free-atom ground-state functions (B $1s^2 2s^2 2p^1$ and N $1s^2 2s^2 2p^3$) or the wave functions corresponding to singly ionized atoms produce too large values of the low-momentum Compton components.

D. X-ray scattering factors

X-ray scattering factors provide through the Fourier transform of the charge density, a direct measure of the ground-state electronic charge distribution in the solid. First-principles calculations of this quantity for diamond and boron nitride are particularly interesting because: (i) The (222) reflection, called "forbidden" for diamond is zero for a homonuclear tetrahedral compound when the crystal density is assumed to be given by a superposition of spherical atomic densities. Its determination furnishes a direct measure of the deviation of the crystal density from spherical symmetry around each atomic site. (ii) The magnitude of the (200) reflection in BN (absent in diamond) yields an important measure of the asymmetry of the charge density since it corresponds to the difference in the single-site atomic structure factors.

Table II presents the x-ray scattering factors obtained in the present exchange and correlation model, the observed values,¹⁷ the results of Euwema *et al.*²⁷ obtained in a crystalline Hartree-Fock model, and, for comparison, the values obtained by a simple superposition model.

The main conclusions that can be drawn from this study are: (i) The difference between the values of the (222) reflection calculated in the direct crystal and atomic superposition models is somewhat smaller in BN than that obtained in diamond (0.10e

and $0.14e$,⁵³ respectively) and indicates a somewhat smaller nonspherical character of the site charge distribution in BN. (ii) The strong (200) reflection observed in BN suggests substantial charge polarization in this system. However, the rough agreement with this value obtained already from a superposition of neutral atom densities indicates that actual large charge transfer between the two sublattices (as opposed to overlap of the corresponding wave function) cannot be inferred from the size of the observed reflection. (iii) The local density calculation of the scattering factor is in very good agreement with experiment; for almost all reflections, the agreement is within experimental error. By contrast, the HF crystal results do not show the same degree of agreement. It is noted however that our calculated value for the (222) reflection is somewhat too high, indicating that our LDF representation of the crystal density is too anisotropic, relative to the superposition limit.

E. Behavior under pressure and cohesive properties

To simulate the effect of pressure, we have calculated the band structure for a series of 9 different lattice constants between 3.40 and 3.85 Å. The calculated results shown in Fig. 11 indicate that the band levels can be grouped into three categories according to their behavior:

(a) The energies of the valence bands decrease substantially with decreasing lattice constant and follow different slopes for the various band states. There appears to be a direct correlation between the amount of 2s character in these bands and their pressure derivative: in the lower valence band (VB1) the pressure derivative [defined as $(d\epsilon/dp) = -K(d\epsilon/d\ln V)$], with the volume compressibility K approximately 0.24×10^{-12} dyn/cm²]³ ranges from 5.4×10^{-6} eV/bar at $\Gamma_{1,\nu}$ (54% N 2s and 46% B 2s) to 3.6×10^{-6} eV/bar at $X_{1,\nu}$ (64% N 2s, 0% B 2s). For the higher group of valence bands (VB2) which have substantially less 2s character (cf. Fig. 8), the pressure derivative ranges between 2.3×10^{-6} and 3.6×10^{-6} eV/bar. This behavior stems from the stronger lattice constant dependence of the 2s Hamiltonian matrix elements compared with the 2p elements. Denoting such a dependence by $H_{\mu\nu}^{\alpha\beta}(\vec{k}) \sim A R^{-n}$ where μ, ν denote Bloch orbitals and α, β denote atoms, we find at Γ $n \approx 5.4$ for $H_{2s,2s}^{B,B}$, $n \approx 4.0$ for $H_{2s,2s}^{N,N}$, and $n \approx 4.8$ for $H_{2p,2p}^{BN}$ compared with $n=0.5$ and $n=0.2$ for $H_{2p,2p}^{B,B}$ and $H_{2p,2p}^{N,N}$ respectively. The B-B interaction is somewhat more sensitive to lattice constant variation than are the N-N elements due to the larger extent of the B 2s orbitals (the overlap of Bloch basis functions at Γ are $S_{2s,2s}^{B,B} = 3.6$ and $S_{2s,2s}^{N,N} = 1.7$). Note that the lattice

TABLE II. X-ray scattering factors of boron nitride; "sup" indicates the results of a superposition of spherical (neutral) atomic densities while "band" indicates those from a crystalline calculation.

(h k l)	HF _{sup} ^a	LDF _{sup}	HF _{band} ^b	LDF _{band}	Expt. ^a
1 1 1	4.62	4.42	5.05	4.97	4.92 ± 0.15
2 0 0	1.40	1.49	1.56	1.58	1.56 ± 0.05
2 2 0	4.21	4.14	4.10	4.17	4.17 ± 0.10
3 1 1	2.69	2.60	2.52	2.64	2.59 ± 0.10
2 2 2	0.48	0.47	0.44	0.57	0.50 ± 0.02
4 0 0	3.30	3.25	3.20	3.20	3.22 ± 0.10
3 3 1	2.17	2.18	2.22	2.16	2.17 ± 0.05
4 2 0	0.29	0.36	0.28	0.32	0.32 ± 0.01
5 1 1	1.90	1.96	1.97	1.95	1.96 ± 0.06
3 3 3	1.90	1.96	...	1.97	1.96 ± 0.06

^aHartree-Fock superposition model, Ref. 17.

^bHartree-Fock superposition model, Ref. 27.

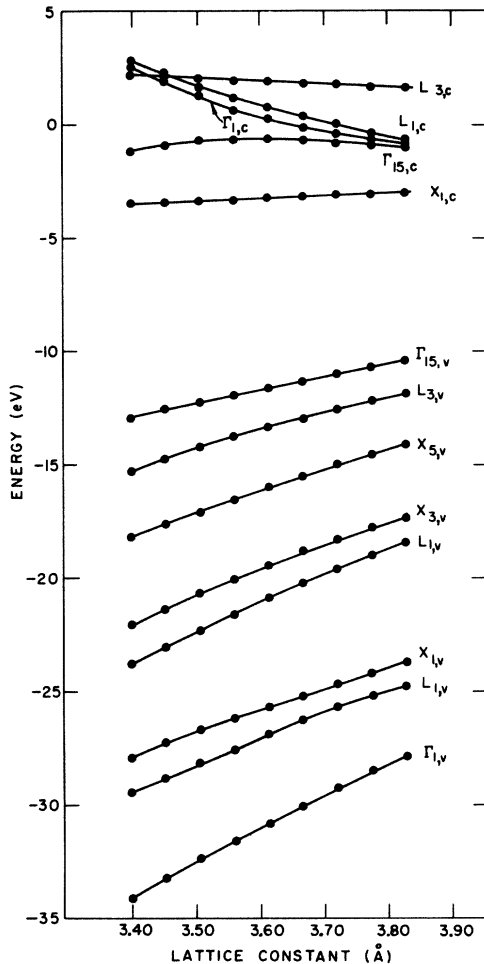


FIG. 11. Lattice constant dependence of the band energies in cubic BN. Full dots indicate calculated points.

constant variation of the valence band eigenvalues is substantially stronger than that anticipated for an ionic material (in which this dependence follows essentially that of the Madelung potential⁵⁴ due to the importance of the covalent overlap terms.

(b) The lower conduction band states (e.g., X_{1c} , Γ_{15c}) show a very small decrease in energy with lowering of the lattice constant which originates from a combination of two effects: the small hybridization of N character into these predominantly B $2p$ states introduces a partial cancellation in the electrostatic Madelung terms of the oppositely charged sublattices (this effect is particularly strong in pure ionic materials such as LiF).⁵⁴ In addition, the overlap between the B $2p$ Bloch functions and B and N $2p$ Bloch functions is very small (0.36 and 0.07, respectively) and results in a very weak lattice constant dependence.

(c) The higher conduction states (Γ_{1c} and L_{1c}) show a strong increase in energy with decreasing

lattice constant on account of their pronounced B $2s$ antibonding character. The substantial B-B $2s$ overlap (≈ 3.6) makes these states particularly sensitive to lattice constant variations.

To our knowledge, the pressure behavior of the transition energies in BN have not been measured. Such measurements would be particularly interesting in this system in view of the variations predicted here (e.g., about 10×10^{-6} eV/bar for the $\Gamma_{15,v} \rightarrow \Gamma_{1c}$ transition and 0.2×10^{-6} eV/bar for the indirect gap $\Gamma_{15,v} \rightarrow \Delta_{\min}$ transition) and the bearing they have on the bonding picture in this material.

Finally, we compare the major difference in lattice constant behavior between our results for BN and our previous results for diamond.⁵ We find that the pressure dependence of *valence* states is somewhat weaker in diamond than in BN (e.g., a pressure coefficient of 3.1×10^{-6} eV/bar for the $\Gamma_{1,v}$ state in diamond as compared with 5.4×10^{-6} eV/bar in BN) while the reverse is true for the *conduction* bands. (This probably stems from the fact that the carbon-carbon interactions are intermediate between the B-B and the N-N interactions and from the lack of electrostatic Madelung-type terms in homopolar diamond). The interband $\Gamma_{15,v} \rightarrow \Gamma_{1c}$ transition is predicted to have a pressure coefficient which is about 15 times larger than that for the $\Gamma_{15,v} \rightarrow X_{1c}$ transition in BN, while in diamond the analogous transitions ($\Gamma_{25,v} \rightarrow \Gamma_{1c}$ and $\Gamma_{25,v} \rightarrow X_{1c}$) are predicted to be only 7 times larger. It is interesting to observe that whereas our calculation for BN indicates an interchange in position of the L_{1c} and L_{3c} bands with a 4% reduction of the equilibrium lattice constant, the same crossing in diamond appears at a much smaller reduction in the equilibrium lattice constant (about < 1%).

We close this section by considering the cohesive properties of BN. We have calculated the total crystal energy per unit cell directly from the band charge density, by the method previously described.^{9,10} Repeating this calculation for five values of the lattice parameters between 3.50 and 3.73 Å and interpolating, we find a minimum in the total energy E_t at $a_{\text{eq}} = 3.652$ Å of $E_t = -2149.035$ eV/pair. The observed room-temperature lattice constant of BN is 3.6157 Å^{1,17}; the value extrapolated to 0 K is³ 3.615 Å and hence only 1% smaller than our result. To obtain the cohesive (binding) energy of BN (relative to ground state neutral atoms), we subtract from E_t the sum of atomic total energies obtained by Gunnarsson⁵⁵ in a spin-polarized local-spin-density formalism⁵⁶ which yields in the non-spin polarized limit the same functional used here for the closed shell solid³¹ ($E_t^{\text{B}} = -662.9009$ and $E_t^{\text{N}} = -1473.3344$ eV) to yield a value of 12.8 ± 0.5 eV/pair. [Our estimated theoretical uncertainty in the

binding energy (mainly due to the slow convergence of the total energy integrals with the number of Diophantine points) is 0.5 eV.] The experimental value for this quantity is estimated to be 13 eV/pair.⁵⁷ [In our previous study on diamond we obtained, using Gunnarsson's atomic calculations,⁵⁵ a binding energy of 15.6 eV/pair (experimental: 15.2 eV/pair and an equilibrium lattice constant of 3.581 Å (experimental: 3.567 Å).] The agreement between our calculated results and experiment is

rather good. Further, the observed trend in going from diamond to the more ionic BN (decrease in cohesive energy and increase in equilibrium lattice constant) are reproduced remarkably well.

ACKNOWLEDGMENT

Part of these computations were performed at the ASD Computer Center, Wright-Patterson, Dayton, Ohio. We are grateful to the staff for their cooperation.

*Supported by the NSF (through the Materials Research Center, Northwestern University), and the Air Force Office of Scientific Research.

†Present address: Department of Physics, University of California, Berkeley, California 94709.

- ¹R. H. Wentorf, *J. Chem. Phys.* **26**, 956 (1957); *ibid.* **34**, 809 (1961).
- ²P. Grodzinski *Nature* **177**, 1828 (1956); N. A. Goryunova, A. S. Borschevskii, and D. N. Tretiakov in *Semiconductors and Semimetals*, edited by R. K. Willardson and A. C. Beer (Academic, New York, 1968), Vol. 4, p. 7.
- ³P. J. Gielisse, S. S. Mitra, J. N. Plendl, R. D. Griffis, L. C. Mansur, R. Marshall, and E. A. Pascoe, *Phys. Rev.* **155**, 1039 (1967).
- ⁴G. Lucovsky, R. M. Martin and E. Burstein, *Phys. Rev. B* **4**, 1367 (1971).
- ⁵A. Zunger and A. J. Freeman, *Phys. Rev. B* **15**, 5049 (1977).
- ⁶A. Zunger and A. J. Freeman, *Phys. Lett.* **57A**, 453 (1976).
- ⁷P. Hohenberg and W. Kohn, *Phys. Rev. B* **6**, 164 (1964).
- ⁸W. Kohn and L. J. Sham, *Phys. Rev.* **140**, 1133 (1965).
- ⁹A. Zunger and A. J. Freeman, *Phys. Rev. B* **15**, 7716 (1977).
- ¹⁰A. Zunger and A. J. Freeman, *Int. J. Quant. Chem. S* **10**, 383 (1976).
- ¹¹R. M. Chrenko, *Solid State Commun.* **14**, 511 (1974).
- ¹²H. R. Philipp and E. A. Taft, *Phys. Rev.* **177**, 159 (1967).
- ¹³A. Halperin and A. Katzir, *J. Phys. Chem. Solids* **36**, 89 (1975).
- ¹⁴V. V. Nemoshkalenko and V. G. Aleshiu, *Fiz. Tver. Tela* **12**, 59 (1970) [*Sov. Phys.-Solid State* **12**, 46 (1960)].
- ¹⁵V. A. Formichev, *Bull. Acad. Sci. USSR, Phys. Ser.* **31**, 972 (1967).
- ¹⁶V. A. Formichev and M. A. Rumsh, *J. Phys. Chem. Solids* **29**, 153 (1972).
- ¹⁷R. J. Weiss, *Philos. Mag.* **29**, 1029 (1974); *ibid.* **26**, 153 (1972).
- ¹⁸L. Kleinman and J. C. Phillips, *Phys. Rev.* **117**, 460 (1960).
- ¹⁹J. C. Phillips, *J. Chem. Phys.* **48**, 5740 (1968).
- ²⁰C. A. Coulson, L. B. Redei, and D. Stocker, *Proc. R. Soc.* **270A**, 357 (1962).
- ²¹L. B. Redei, *Proc. R. Soc.* **270A**, 383 (1962).
- ²²F. Bassani and M. Yoshimine, *Phys. Rev.* **130**, 20 (1963).
- ²³D. R. Wiff and R. Keown, *J. Chem. Phys.* **47**, 3113 (1967).
- ²⁴R. Keown, *J. Chem. Phys.* **48**, 5741 (1968).
- ²⁵V. G. Aleshin, V. P. Smirnov, and B. V. Gantesvich, *Fiz. Tver. Tela* **10**, 2884 (1968) [*Sov. Phys.-Solid State* **10**, 2282 (1969)].
- ²⁶L. A. Hemstreet and C. Y. Fong, *Phys. Rev. B* **6**, 1464 (1972).
- ²⁷R. N. Euwema, G. T. Surratt, D. L. Wilhite, and G. G. Wepfer, *Philos. Mag.* **29**, 1033 (1974).
- ²⁸R. N. Euwema and D. J. Stukel, *Phys. Rev. B* **1**, 4692 (1970).
- ²⁹A. Zunger, A. Katzir, and A. Halperin, *Phys. Rev. B* **5**, 5560 (1976).
- ³⁰A. Zunger, *J. Phys. C* **6**, 76 (1974); **6**, 96 (1974).
- ³¹K. S. Singwi, A. Sjölander, P. M. Tosi, and R. J. Land, *Phys. Rev. B* **1**, 1044 (1970).
- ³²P. P. Ewald, *Ann. Physik.* **64**, 253 (1921).
- ³³C. B. Haselgrove, *Math. Compt.* **15**, 373 (1961); G. S. Painter and D. E. Ellis, *Phys. Rev. B* **1**, 4727 (1970).
- ³⁴D. J. Chadi and M. L. Cohen, *Phys. Rev. B* **8**, 5747 (1973).
- ³⁵R. C. Chaney, C. C. Lin, and E. E. Lafon, *Phys. Rev. B* **3**, 459 (1971).
- ³⁶D. M. Drost and J. L. Fry, *Phys. Rev. B* **2**, 7887 (1970).
- ³⁷F. Herman, *J. Electron. Phys.* **1**, 103 (1955).
- ³⁸W. Baronian, *Mater. Res. Bull.* **7**, 119 (1972).
- ³⁹J. C. Phillips, *Solid State Physics*, edited by F. Seitz and D. Turnbull (Academic, New York, 1966), p. 756.
- ⁴⁰A. A. Levin, *Fiz. Tekh. Poluprovod.* **5**, 1481 (1971) [*Sov. Phys.-Semicond.* **5**, 1297 (1972)].
- ⁴¹R. S. Mulliken, *J. Chem. Phys.* **26**, 792 (1952).
- ⁴²P. O. Löwdin, *J. Chem. Phys.* **18**, 365 (1950).
- ⁴³S. Ciraci, *Phys. Status Solidi* **706**, 689 (1975).
- ⁴⁴S. T. Pantelides and W. A. Harrison, *Phys. Rev. B* **11**, 3006 (1975).
- ⁴⁵E. W. Stout and P. Politzer, *Theor. Chim. Acta* **12**, 379 (1968); B. J. Duke, *Theor. Chim. Acta* **9**, 710 (1968).
- ⁴⁶A. Neckel, P. Rastl, R. Eibler, P. Weinberger, and K. Schwarz, *J. Phys. C* **9**, 579 (1976).
- ⁴⁷K. H. Johnson and F. C. Smith, in *Computational Methods in Band Theory*, eds. P. M. Marcus, J. F. Janak, and A. R. Williams, (Plenum, New York, 1971) p. 377.
- ⁴⁸A. A. Maradudin, E. W. Montrol, G. H. Weiss, and I. P. Ipatova *Theory of Lattice Dynamics in the Harmonic Approximation* (Academic, New York, 1971).
- ⁴⁹B. I. Bennett and A. A. Maradudin, *Phys. Rev. B* **5**, 4146 (1972).

- ⁵⁰M. B. Khusidman and V. S. Neshpor, *Poroshk. Metall.* **8**, 72 (1970).
- ⁵¹J. L. Masse, *Helv. Chim. Acta* **47**, 314 (1964).
- ⁵²Z. J. Kuplyauskis and I. A. Yakimavichyus, *Fiz. Tverd. Tela* **16**, 1832 (1975). [*Sov. Phys.-Solid State* **16**, 1832 (1975)].
- ⁵³M. Renninger, *Acta Cryst.* **8**, 606 (1955).
- ⁵⁴A. Zunger and A. J. Freeman, *Bull. Am. Phys. Soc.* **22**, 410; and *Phys. Rev. B* (to be published).
- ⁵⁵O. Gunnarsson (private communication).
- ⁵⁶O. Gunnarsson and B. I. Lundqvist, *Phys. Rev. B* **13**, 4274 (1976); O. Gunnarsson, B. I. Lundqvist, and S. Lundqvist, *Solid State Commun.* **11**, 149 (1971).
- ⁵⁷The cohesive energy of cubic BN can only be roughly estimated from the available experimental data. The heat of formation from gaseous N₂ and crystalline boron was determined [A. S. Dworkin, D. J. Sasmur, and E. R. Van Artsdalen, *J. Chem. Phys.* **22**, 837 (1954). See also G. Berl and W. E. Wilson, *Nature* **191**, 380 (1961)] to be 60.7 ± 0.7 kcal/mole at 298 K. Correcting for the atomization energy of nitrogen and boron [L. Pauling, *The Nature of the Chemical Bond* (Cornell University, Ithaca, N.Y. 1960)], for cooling to 0 °K [data from JANAF Tables of Thermochemical Data, edited by D. R. Stull, (Midland, Michigan, 1965)] and finally for the zero-point energy of the solid [using a Debye equation with $\Theta_D = 1700$ K, data given by P. J. Gielisse, S. S. Mitra, J. N. Plendl, R. D. Griffis, L. C. Mançur, R. Marshall, and E. A. Pascoe, *Phys. Rev.* **155**, 1039 (1967)] one obtains an estimate of 13 eV/pair for the static binding energy. The accuracy of this quantity is at present difficult to assess.